
MULTI-SCALE TOPOLOGY OPTIMIZATION USING NEURAL NETWORKS

A PREPRINT

Hongrui Chen¹, Xingchen Liu², and Levent Burak Kara¹

¹ Department of Mechanical Engineering, Carnegie Mellon University

² Intact Solutions

ABSTRACT

A long-standing challenge is designing multi-scale structures with good connectivity between cells while optimizing each cell to reach close to the theoretical performance limit. We propose a new method for direct multi-scale topology optimization using neural networks. Our approach focuses on inverse homogenization that seamlessly maintains compatibility across neighboring microstructure cells. Our approach consists of a topology neural network that optimizes the microstructure shape and distribution across the design domain as a continuous field. Each microstructure cell is optimized based on a specified elasticity tensor that also accommodates in-plane rotations. The neural network takes as input the local coordinates within a cell to represent the density distribution within a cell, as well as the global coordinates of each cell to design spatially varying microstructure cells. As such, our approach models an n -dimensional multi-scale optimization problem as a $2n$ -dimensional inverse homogenization problem using neural networks. During the inverse homogenization of each unit cell, we extend the boundary of each cell by scaling the input coordinates such that the boundaries of neighboring cells are combined. Inverse homogenization on the combined cell improves connectivity. We demonstrate our method through the design and optimization of graded multi-scale structures.

1 INTRODUCTION

There has been a recent increase in machine learning-driven topology and multi-scale structures optimization approaches, particularly using neural networks for performing structural optimization. Both data-driven [1, 2, 3, 4, 5] and direct training-based [6, 7, 8, 9, 10, 11] approaches have been explored. Data-driven approaches typically require large training sets and long training times. They perform instant optimal topology generation during inference time. Direct training approaches use the neural network to represent the density field of a single or a group of designs. Prior works on direct training approaches focus on using the neural network with spatial coordinates as input and density as the output to represent the geometry [9, 10, 6]. Inverse homogenization refers to the optimization of microstructure with the desired property [12]. Sridhara et al. [10] applied direct neural network-based inverse homogenization in designing single microstructure cells. Unfortunately, no direct neural network-based optimization for multi-scale structures has been developed. One key challenge from microstructure design to multi-scale structure is ensuring good connectivity between cells [12]. Connecting individual optimized microstructure cells into a multi-scale structure is called de-homogenization [12]. Cell rotation is included in de-homogenization in which cells can perform very close to the theoretical limit [12]. De-homogenization is a post-processing step to obtain a well-connected multi-scale design introduced by Pantz and Trabelsi [13]. During inverse homogenization, connectivity can also be encouraged where Garner et al. [14] combined adjacent cells and Liu et al. [15] formulated a constraint on the boundary of each cell. However, these previous methods did not incorporate rotation during inverse homogenization. On the other hand, de-homogenization relies on post-processing to add rotation.

In this work, we aim to use a neural network to represent the design of a multi-scale structure such that connectivity and rotation are enforced. We configure a neural network to take in both local and global spatial coordinates to represent multi-scale structural designs. We focus on 2D multi-scale structures, hence the coordinates are two-

dimensional. The local coordinates represent the fine-scale microstructure. The global coordinates correspond with the coarse-scale cell location. Given the local and global coordinate pairs as input, the neural network outputs the density for that specific location as a value between 0 and 1. During training¹, the microstructure for each cell is optimized to maximize or minimize a specific material property, derived from the elasticity tensor. This is often referred to as inverse homogenization [16]. We extend the unit cell boundary to its neighboring cells during inverse homogenization to encourage connectivity between cells. Since the inputs to the neural network are spatial coordinates, transformation matrices, for example, scaling, and rotation, can be applied to the coordinates. We apply rotation matrices to the local input coordinates such that the cell is oriented similarly to de-homogenization[13]. The difference is that in our approach the orientation of the cell is co-optimized during the training of the neural network instead of a post-processing step.

In the training of a conventional machine learning model, a loss function is used to back-propagate and update the parameters in the model. Similarly, we also formulate a combined loss function for the optimization of multi-scale structures. The combined loss includes the target volume fraction for each cell, the error w.r.t target material property, and an L1 loss between cell boundaries to encourage microstructure connectivity. Since the inputs to the neural network are local and global coordinates, one can sample the coordinates at any point in the domain without interpolation. During the optimization, we sample the coordinates at regular intervals which corresponds to the square element used in Finite Element Analysis (FEA). The FEA module operates separately from the machine learning pipeline but outputs the objective value during forward propagation and sensitivities during backpropagation. During the training of the neural network, the network gradually learns the local geometry of each microstructure cell. Once training is finished, we can sample the coordinates at the same or finer interval such that a higher resolution result with smooth and crisp boundary can be obtained.

Our main contributions are:

- a neural network-based optimization of multi-scale structure
- a method to enforce connectivity for multi-scale design
- accommodate rotation of cells with neural network geometry representation

2 RELATED WORK

Multi-scale topology optimization: Multi-scale structures offer the potential to deliver outstanding performance, being inherently lightweight, durable, and versatile. Bendsøe and Kikuchi [17] introduced the homogenization approach for topology optimization. The SIMP method [18, 19] considers the relative material density in each element of the Finite Element (FE) mesh as design variables, allowing for a simpler interpretation and optimized designs with more clearly defined features. A comprehensive review by Wu et al. [12] discusses the existing approaches of multi-scale topology optimization and analysis of their strength and applications. Research that targets improving the compatibility of multi-scale structures includes Garner et al. [14] where adjacent cells were combined when inverse homogenization is performed such that compatibility can be improved. However, adding neighboring cells to the optimization will increase the computation time for FE analysis. We instead extend the cell boundary into neighboring cells where the FE resolution remains the same. Liu et al. [15] formulated a constraint on the boundary of each cell such that given n types of desired microstructure, all these n types share the same boundary. This allows the optimized cell designs to be mutually compatible. One possible limitation is that the total types of cell designs are limited and as the number of cell designs increases, the restriction on the boundary can be increased. In this work, we establish connectivity between neighboring cells, where the limitation on geometry is less. Connectivity is also important when designing multi-scale structures given a material exemplar. Senhora et al. [20] use spinodal architected materials to place material along principal stress directions. A library of microstructure can be pre-generated and connectivity between cells can be improved through mapping [21]. However, the microstructure performance gamut can be limited by the generated dataset.

Direct topology optimization with neural networks: We refer to direct topology optimization methods as those that do not use any prior data but rather train a neural network in a self-supervised manner for learning the optimal density distribution/topology. Chandrasekhar and Suresh [6] explored a direct approach where the density field is parameterized using a neural network. The direct approach has also been extended to designing microstructure cells [10]. We further extend upon single-cell design to formulate a neural network for graded multi-scale structure design.

Fourier projection-based neural network for length scale control [8] and application for multi-material topology optimization [7] has also been explored. Deng and To [22] propose topology optimization with Deep Representation

¹Here “training” refers to optimization and back-propagation. Training has been used in previous related works [6, 11] but this is different from data-driven machine learning

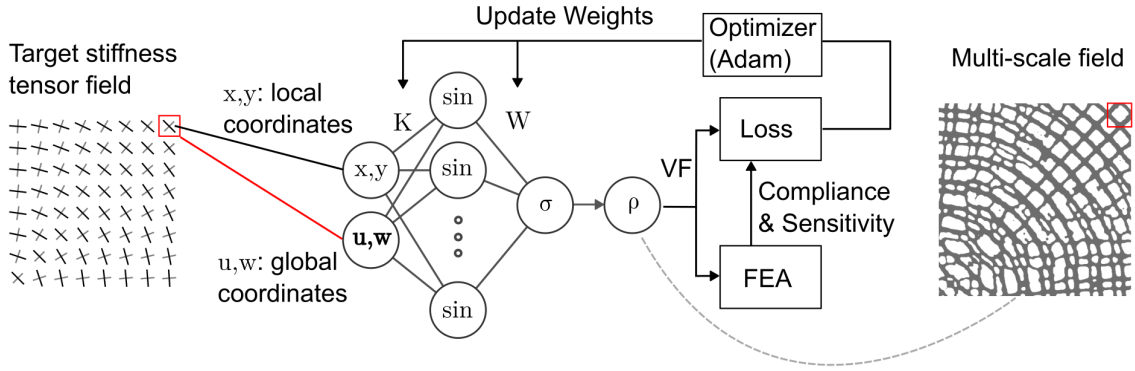


Figure 1: The neural network outputs density ρ at each coordinate point. By sampling coordinate points across the design domain, we obtain the density field. From the density field, we calculate the current volume fraction and the homogenized stiffness tensor from an FEA solver. The homogenized stiffness tensor and volume fraction are then formulated as a loss function which is used in backpropagation of the training process until convergence.

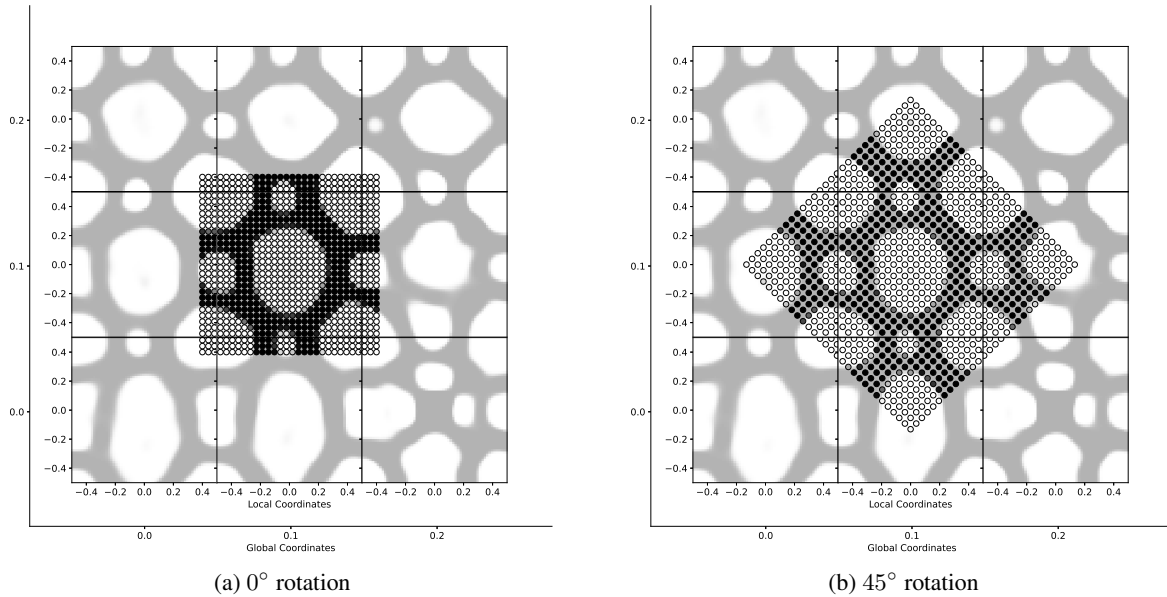
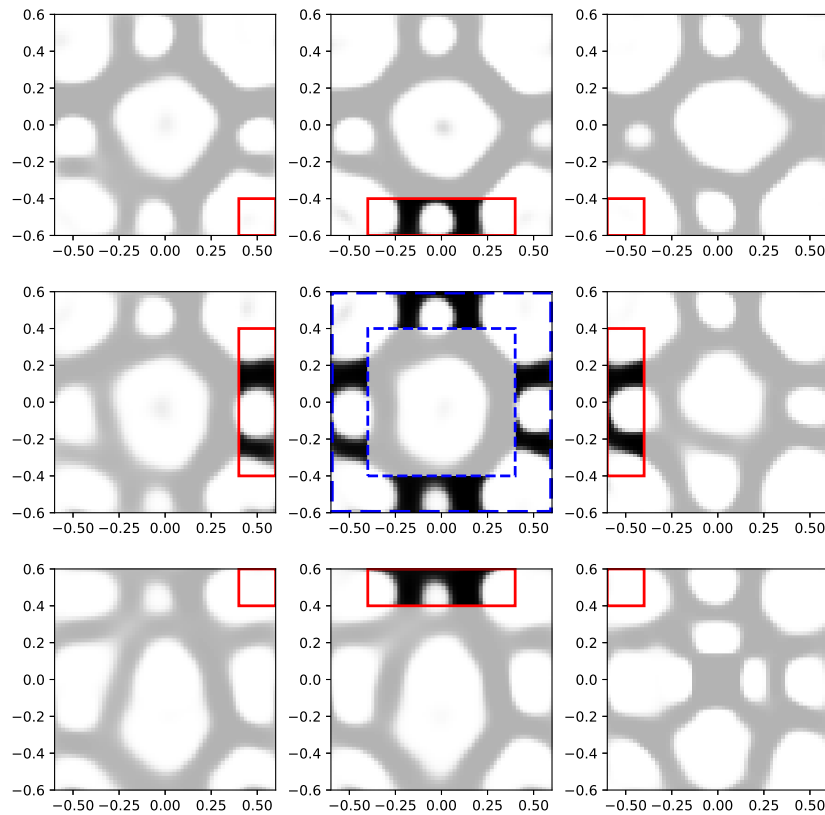
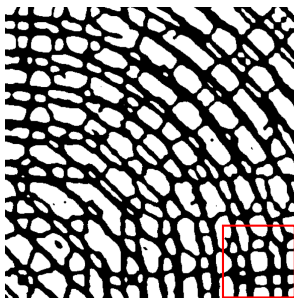


Figure 2: Sampling inside the continuous topology domain for finite element analysis. When the rotation is at 0° , the boundary is extended by 1.2 times to ensure all 8 neighboring cells are covered. With a 45° rotation, a 1.6 times increase is applied.

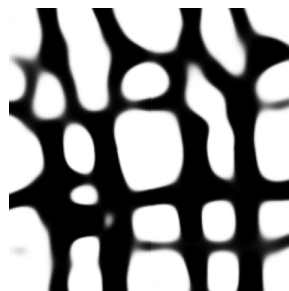
Learning, with a similar concept of re-parametrization, and demonstrate the effectiveness of the proposed method on minimum compliance and stress-constrained problems. Deng and To [23] also propose a neural network-based method for level-set topology optimization, where a fully connected deep neural network describes the implicit function of the level-set. Zehnder et al. [11] effectively leverage neural representations in the context of mesh-free topology optimization and use multilayer perceptrons to parameterize both density and displacement fields. It enables self-supervised learning of continuous solution spaces for topology optimization problems. Mai et al. [24] develop a similar approach for the optimum design of truss structures. Hoyer et al. [25] use CNNs for density parametrization and directly enforce the constraints in each iteration, reducing the loss function to compliance only. They observe that the CNN solutions are qualitatively different from the baselines and often involve simpler and more effective structures. Zhang et al. [26] adopt a similar strategy and show solutions for different optimization problems including stress-constrained problems and compliant mechanism design.



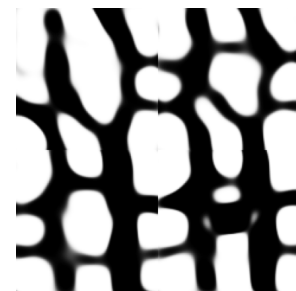
(a) Graphical illustration of boundary loss regions



(b) Multi-scale structure



(c) With boundary loss



(d) Without boundary loss

Figure 3: The boundary loss is defined as the L1 loss between the red solid line region and the blue dashed line region in (a). When we zoom into the right bottom corner of the multi-scale structure shown in (b), we can observe that with boundary loss (c), the connection between cells is more continuous when upsampled compared to without boundary loss (d).

3 PROPOSED METHOD

In our proposed method, the density distribution of the multi-scale structure is directly represented by the topology neural network.

3.1 Neural network-based topology representation

The topology network $T(\mathbf{X})$ (Figure 1), learns a density field differently as compared to typical topology optimization which represents the density field as a finite element mesh. The topology neural network takes in local domain coordinates x, y , as well as the global coordinate u, w for each cell. The global coordinates get concatenated with the local coordinates to form the input to the topology network, $\mathbf{X} = [x, y, u, w]$. The local coordinates are normalized between -0.5 to 0.5 . The global coordinates are normalized between -0.5 to 0.5 along the longest axis. Given the local and global coordinates, the topology network outputs the density value ρ at each coordinate point. The domain coordinates represent the center of each element in the design domain. During topology optimization, a batch of domain coordinates that correspond to the mesh grid and the corresponding strain energy field is fed into the topology network. The output is then sent to the FE solver. The solver outputs the compliance which is combined with the volume fraction violation as a loss. The loss is then backpropagated to learn the weights of the topology network.

We implement the neural network in TensorFlow. For the topology network design, we employed a simple architecture that resembles the function expression of $f(x) = \mathbf{w} \sin(\mathbf{K}x + \mathbf{b})$. Similar neural network architectures have been used to control the length scale of geometry in topology optimization[8]. The conditioned domain coordinates are multiplied with a kernel \mathbf{K} . The kernel \mathbf{K} regulates the frequency of the sine function. We add a constant value of 1 to break the sine function’s rotation symmetry around the origin. We use a Sigmoid function to guarantee the output is between 0 and 1. The topology network can be formulated as follows:

$$T(\mathbf{X}) = \sigma(\mathbf{W} \sin(\mathbf{K}\mathbf{X} + 1)) \quad (1)$$

where:

\mathbf{X} : Domain coordinate input, $\mathbf{X} = (x, y, u, w)$

σ : Sigmoid activation function

\mathbf{K} : Trainable frequency kernels

\mathbf{W} : Trainable weights

3.2 Multi-scale topology optimization with neural networks

The goal of using the neural network to represent the topology is to enforce compatibility between cells. The compatibility is achieved with the extension of the cell boundaries, which is illustrated in Figure 2. In 2D, we extend the boundary of each cell by 1.2 times to cover all its 8 neighboring cells. If rotation of the cell is required, the boundary is further extended to 1.6 times to cover all 8 neighboring cells. For the extended regions that are in neighboring cells, the domain coordinates use the local and global coordinates for neighboring cells. We use 4 node square elements for finite element analysis. Within the boundary, we sample the domain at uniform intervals that directly correspond with the finite element mesh. During training, the iterative updates to the design domain are carried out on these sampling points.

The second mechanism to encourage cell compatibility is boundary loss. Once we upsample the input coordinate to obtain geometry at finer resolution, we observe that there are still small inconsistent transitions between cell boundaries which can be seen in Figure 3. Therefore, a boundary loss is added to improve the consistency between cells.

The boundary loss is formulated as the L1 loss between the outer edge of the neighboring cells and the outer edge of the center cell.

$$\mathcal{L}_{bc} = \frac{1}{n} \sum^n |T(X_{neigh}) - T(X_{center})| \quad (2)$$

As illustrated in Figure 3, the outer region $T(X_{neigh})$ for the 8 neighboring cells consists of the area highlighted in solid red lines and the outer region for the center cell $T(X_{center})$ is highlighted in blue dashed lines. The extent of the sampling for each cell is also expanded by 1.2 times. For the regular sampling for the continuous multi-scale structure, each local coordinate is normalized between -0.5 and 0.5 . During the computation of the boundary loss, each cell is

further expanded by 1.2 times such that the local coordinates are in the range of -0.6 to 0.6. During the optimization, the boundary loss is turned on after 50 epochs.

During optimization, the topology network outputs the density value at the center for each element. These density values are then sent to the finite element solver to calculate the homogenized stiffness tensor based on the SIMP interpolation. [I see this part could be controversial, especially mixing anisotropy with SIMP. You may want to acknowledge that there are other ways to do this, and explain why you did what you did.] We adopted the educational MATLAB code by Xia and Breitkopf [27] for inverse homogenization and programmed the FE code in Python to connect with the neural network that is implemented in TensorFlow.

$$E_{ijkl} = \frac{1}{|Y|} \sum_{e=1}^N (\mathbf{u}_e^{ij})^T \mathbf{k}_e \mathbf{u}_e^{kl} \quad (3)$$

The homogenization is based on an energy-based approach where unit test strains are directly imposed on the boundaries of the base cell. We note that $11 \rightarrow 1$, $22 \rightarrow 2$, and $12 \rightarrow 3$. A weight w is assigned to each of the components of the stiffness tensor.

$$c = -(w_{11}E_{11} + w_{12}E_{12} + w_{13}E_{13} + w_{22}E_{22} + w_{23}E_{23} + w_{33}E_{33}) \quad (4)$$

The finite element solver is treated as a black box within the neural network. It takes in the density of each element and outputs the homogenized stiffness tensor and the sensitivity for each element with respect to the stiffness tensor. Variables that are being optimized are the weights \mathbf{W} and kernels \mathbf{K} of the neural network. Adam[28] is used to train the neural network. The constrained optimization problem needs to be transferred into an unconstrained minimization problem for neural networks. The combined loss function is

$$\mathcal{L} = \frac{1}{n} \sum \frac{c_i}{c_{0,i}} + \alpha \left(\frac{V_i}{V_i^*} - 1 \right)^2 + \beta \mathcal{L}_{bc,i} \quad (5)$$

The compliance c_i is calculated for each cell i and normalized against the compliance $c_{0,i}$ which is calculated from a homogenized density field with volume fraction of V_i^* . α is the penalty factor volume fraction V_i of each cell i . Starting from the first epoch, it gradually increases to 100 at the end of the optimization. β is the penalty factor for the boundary loss \mathcal{L}_{bc} which remains 0 until epoch 50 and gradually increases to 1 at the end of the optimization. We choose epoch 50 as we can observe some microstructure starts to appear while the domain is still largely not converged. One example of convergence history is plotted in Figure 5. A similar loss function for a single scale has also been used by Chandrasekhar and Suresh [6] for compliance minimization and volume fraction constraint with neural networks.

4 RESULTS AND DISCUSSIONS

We set up problems with varying stiffness tensor targets, changing volume fractions, and rotation of stiffness tensor targets. These problems aim to test the ability of the neural network-based multi-scale optimization to design compatible microstructure. All experiments are run on a PC with i7-12700K as the processor, 32 GB of RAM, and Nvidia RTX3080 GPU.

4.1 Multi-scale topology optimization with varying stiffness tensor

We first evaluate the effectiveness of our approach with changing stiffness tensor targets. The stiffness tensor target is formulated as a combination of varying weights on the compliance calculated for each cell. For example, the bottom left side of Figure 4 targets a stiffness tensor with the ratio of: $\begin{bmatrix} 0.6 & 0.75 & 0.0 \\ 0.75 & 0.6 & 0.0 \\ 0.0 & 0.0 & 0.0 \end{bmatrix}$ is written in as $c = -(0.6E_{11} + 1.5E_{12} + 0.6E_{22})$.

The example in Figure 4 consists of 8x8 cells on the coarse scale, 30x30 elements on the fine scale, and a uniform volume fraction target of 0.4. The stiffness tensor weights are configured such that in the horizontal direction E_{11} is increased. In the vertical direction E_{22} is increased. We run the optimization for 300 epochs and plot out a snapshot of the multi-scale structure during training in Figure 5. The optimization takes 9 minutes to run. During optimization, we observe that cells converge in clusters. On the top right corner of Figure 5 is a large cluster where the cells converged

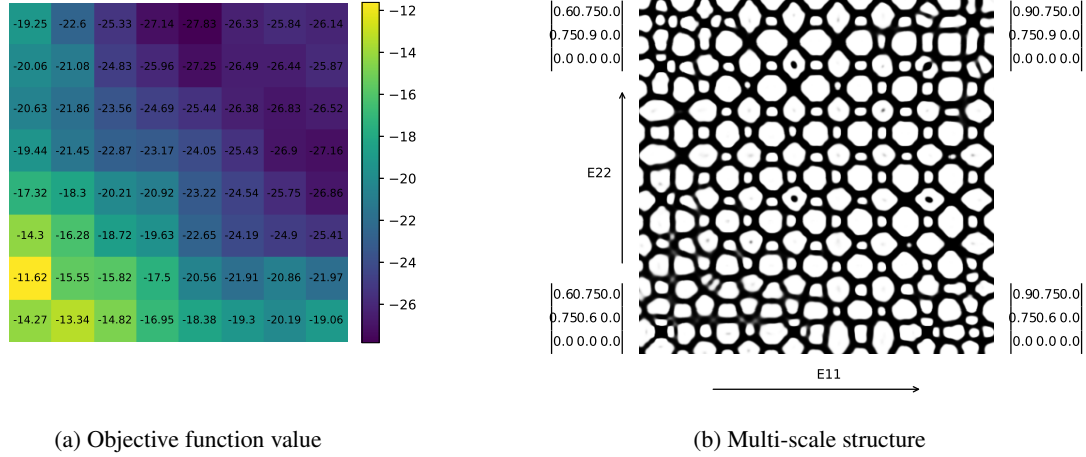


Figure 4: Given a changing stiffness tensor weights, we can observe in (a) that, as the combined weights increase to the top right corner, the objective function value for each cell is also smaller. From the converged multi-scale structure, we can observe good connectivity between the cells.

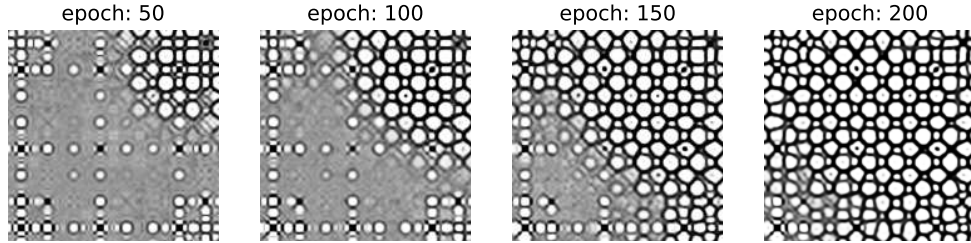


Figure 5: The convergence history of the multi-scale structure from the neural network. Microstructures emerge as clusters and from these clusters gradually propagate through the design domain.

faster. As the optimization progresses, the front with converged microstructure gradually progresses to the bottom left. This could indicate that the neural network is using cells that are closer in global coordinates to interpolate.

In addition to changing the stiffness tensor weights, the volume fraction can also be varied. Compared to the example in Figure 4, the example in Figure 6 has the volume fraction target increasing from 0.3 to 0.5 in the horizontal axis. We can observe the thickness of the multi-scale structure smoothly increased to accommodate for the changing volume fraction. The compliance evaluated in each cell is plotted in Figure 6 (a) where it is lower with a higher volume fraction.

We then configure a problem with varying volume fraction and bulk modulus maximization. This allows us to compare the performance of the theoretical Hashin–Shrickman (HS) upper bound [29]. The converged multi-scale structure is plotted in Figure 7 (b). The volume fraction target in the center is 0.6 and is gradually decreased to 0.4 on the outer edges. We threshold the density field at 0.4. The bulk modulus of each cell and the corresponding HS upper bound are calculated with the thresholded density field. The ratio between the computed bulk modulus versus the HS upper bound is then plotted in 7 (a). On average, across 64 total cells and between 0.4 and 0.56 volume fraction, we achieved 84.9% of the HS upper bound for bulk modulus. This is slightly lower compared to the work by Sridhara et al.[10] where for single microstructure design by the neural network, they achieved 90% of the HS upper bound in the volume fraction range. Slightly higher restrictions on design freedom can be expected with the connectivity constraints posed. We note that no explicit symmetry constraint is applied to this example. The resulting structure demonstrated 2-fold rotation symmetry. While mirror symmetry is missing. This is attributed to the architecture of the neural network.

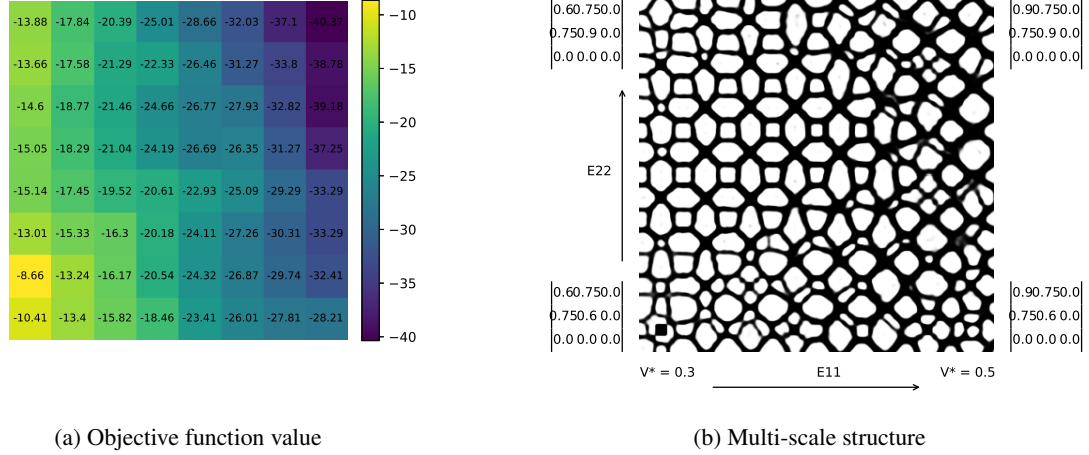


Figure 6: The volume fraction target is varied for each cell along the horizontal direction. Good compatibility is observed as the microstructure edges gradually thicken. The objective value is also lower with higher volume fraction as the stiffness tensor is greater for cells with higher volume fraction.

Inputting global coordinates that are from the I and III or II and IV quadrants leads to the same result. For results where mirror symmetry is desired, explicit mirroring of the global coordinates needs to be performed. Previous works with neural network-based topology optimization also required such mirroring [6].

4.2 Multi-scale topology optimization with cell rotation

The example in 8 (a) consists of a rotated stiffness tensor target of $E_{11} = 1.25E_{22}$. Given a target stiffness tensor field with rotation for example Figure 8 (a), we can either rotate the homogenized stiffness tensor or rotate the geometry. Since the input to the neural network consists of local and global coordinates, we can apply linear transformation matrices to the local coordinates. To rotate the geometry, a 2D rotation matrix can be multiplied on the local coordinates x, y for each cell:

$$\begin{bmatrix} x' \\ y' \end{bmatrix} = \begin{bmatrix} \cos \theta & -\sin \theta \\ \sin \theta & \cos \theta \end{bmatrix} \begin{bmatrix} x \\ y \end{bmatrix} \quad (6)$$

To rotate the stiffness tensor E in Voigt notation requires the rotation matrix R for rotating the basis of the stiffness tensor.

$$R = \begin{bmatrix} \cos^2 \theta & \sin^2 \theta & 2 \cos \theta \sin \theta \\ \sin^2 \theta & \cos^2 \theta & -2 \cos \theta \sin \theta \\ -\cos \theta \sin \theta & \cos \theta \sin \theta & \cos^2 \theta - \sin^2 \theta \end{bmatrix} \quad (7)$$

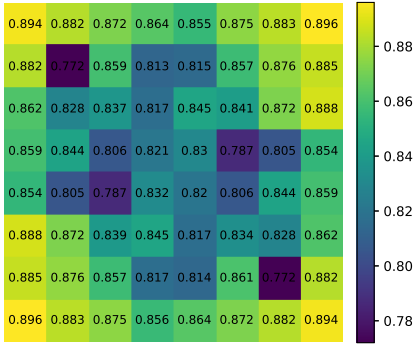
Where the rotation can be applied to the stiffness tensor E with the following equation:

$$E^R = R^{-T} E R \quad (8)$$

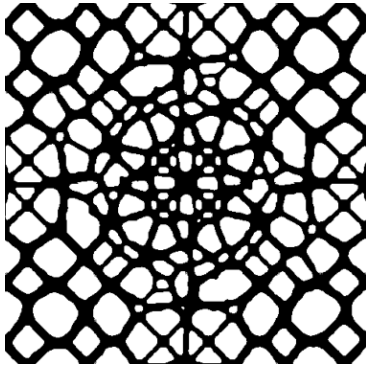
We can then compare the effect of rotating the geometry versus rotating the stiffness tensor. In Figure 8 (b), the geometry is rotated. In Figure 8 (c), the stiffness tensor is rotated. Rotating the geometry leads to microstructure better following the prescribed rotation. The transition is more abrupt in the case of rotating the stiffness tensor. The compliance reached under the same total number of epochs is lower with the rotating of the stiffness tensor.

We can also design multi-scale structures with negative Poisson's ratio material with rotation. The Poisson's ratio is defined as $\mu = \frac{E_{12}}{E_{11} + E_{22}}$. We adopt the relaxed form of compliance objective function proposed in:

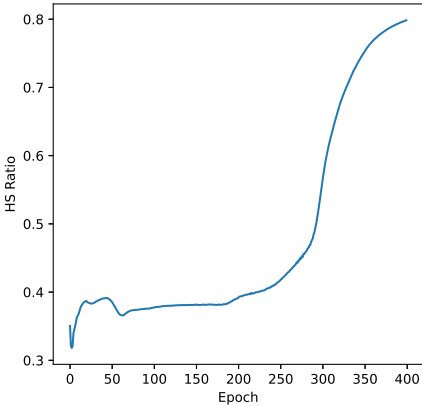
$$c = E_{12} - \beta^l (E_{11} + E_{22}) \quad (9)$$



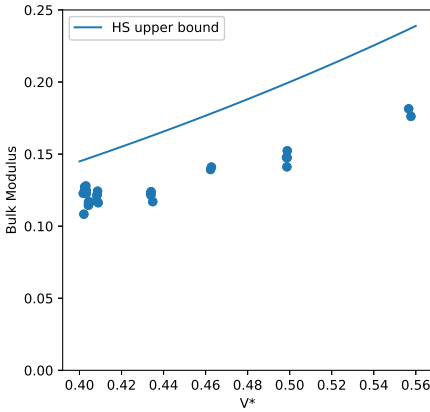
(a) Bulk modulus versus HS upper bound ratio.



(b) Multi-scale structure



(c) Convergence history



(d) Bulk modulus vs volume fraction

Figure 7: We varied the volume fraction between 0.4 to 0.56 and maximized the bulk modulus. Comparing the bulk modulus from the HS upper bound, shown in (a) for each cell, we achieved an average of 84.9%. The convergence history shown in (c) and the bulk modulus vs volume fraction plot in (d) were using the SIMP interpolation of Young’s modules to compare against the HS upper bound. The comparison in (a) uses a binarized density field with volume fraction recalculated for each cell after binarization.

Where l is the design epoch number and $\beta = 0.8$ is chosen such that at the beginning of the optimization, the optimizer tends to maximize the horizontal and vertical stiffness. As the optimization progresses, the optimizer tends to minimize E_{12} , such that materials with negative Poisson’s ratios are generated.

The result of an 8×8 coarse scale, 30×30 element fine scale optimization with rotating microstructure is shown in Figure 9. We can observe that the multi-scale structure is well connected. And evaluating the Poisson’s ratio at each cell, as shown in Figure 9 (a), most of the cells, apart from the center 4 cells, have negative Poisson’s ratio.

4.3 Multi-scale topology optimization with distribution field

In this section, we delve into the utilization of stiffness tensor fields derived from coarse-scale topology optimization. While the previous subsection emphasized the application of smooth rotation and constant stiffness tensor fields, our focus now shifts toward more complicated stiffness tensor fields from coarse-scale topology optimization. The coarse scale topology optimization example shown in Figure 10 (a) consists of a single point load applied on the bottom right. The goal of the coarse-scale optimization is to obtain a principal strain field that can be used as a surrogate stiffness tensor field for subsequent fine-scale optimization. We run the coarse scale optimization at 20×10 resolution with a

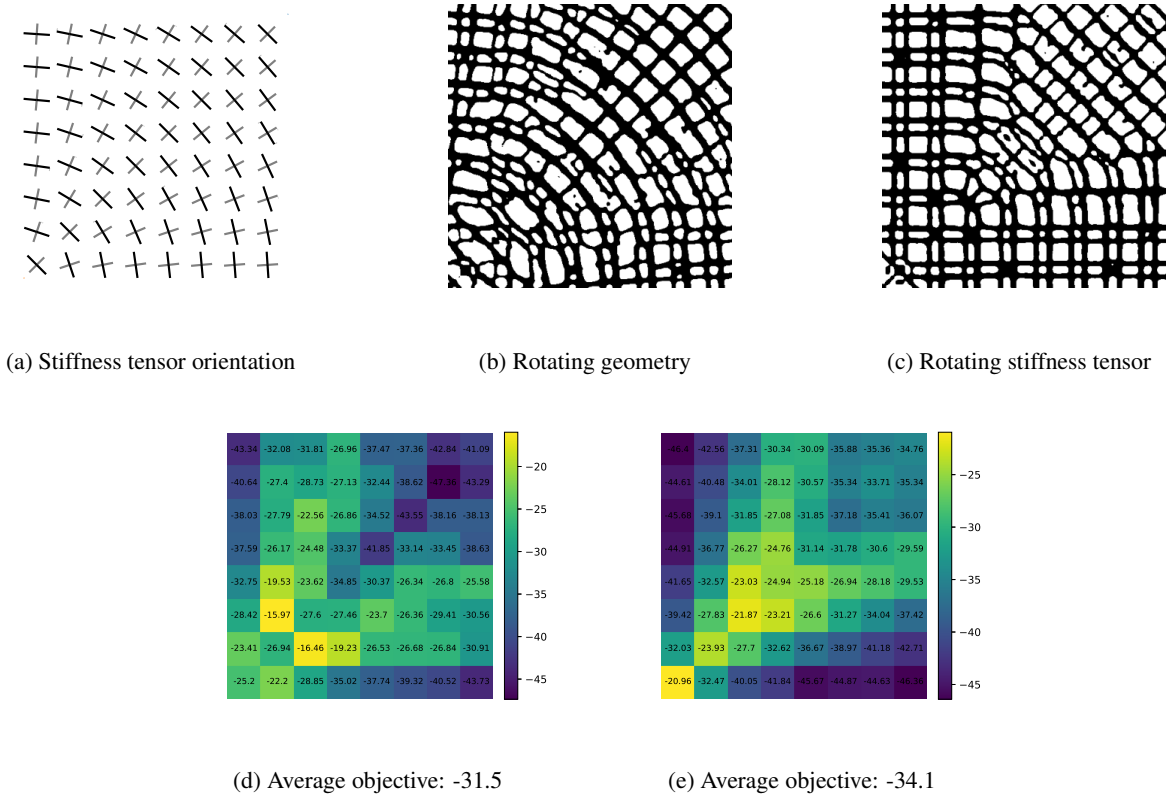


Figure 8: The stiffness tensor field is given in (a). Comparing rotating geometry (b) versus rotating the stiffness tensor (c), rotating the geometry leads to microstructure better following the prescribed rotation. The transition is more abrupt in the case of rotating the stiffness tensor.

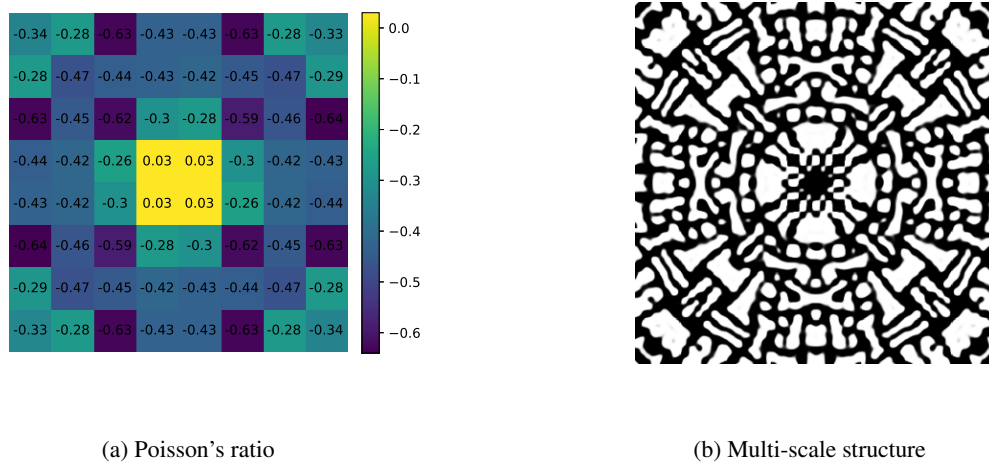
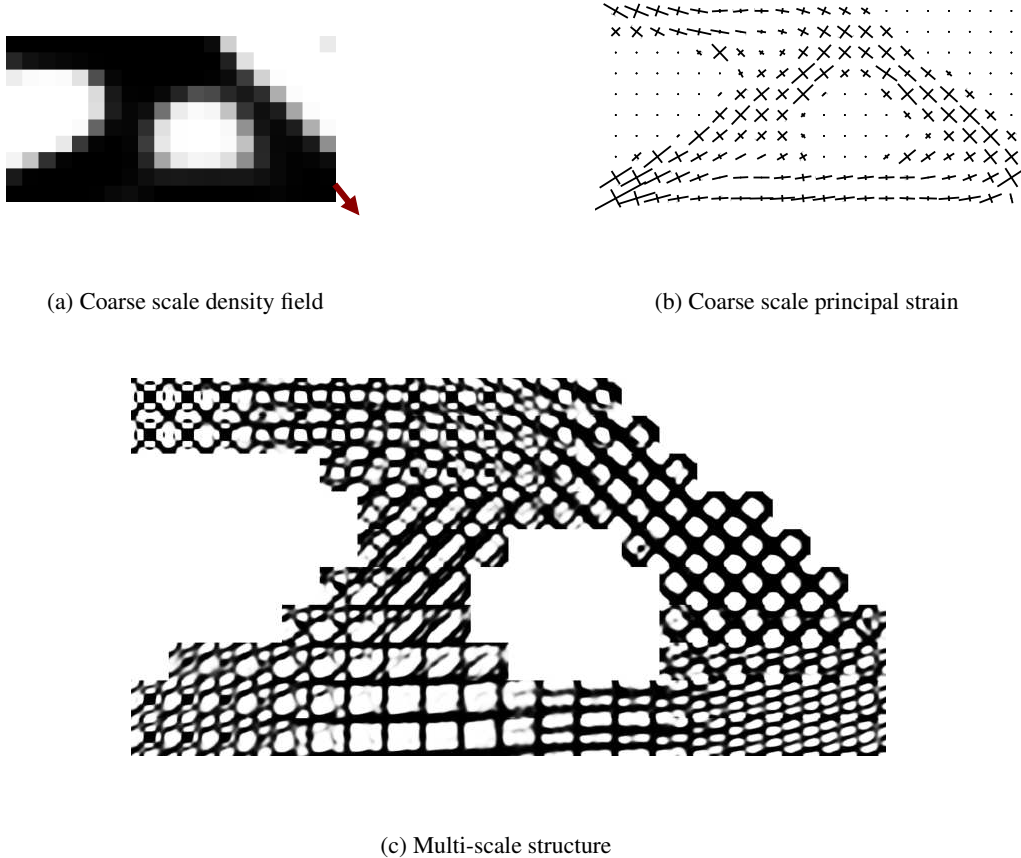


Figure 9: Good connectivity can be observed for this above example where each cell is rotated around the center. Apart from the four center cells', all other cell's Poisson's ratio is negative.



(a) Coarse scale density field

(b) Coarse scale principal strain

(c) Multi-scale structure

Figure 10: We notice a strong connection between the detailed structure and the direction of stiffness. The detailed structures exhibit clustering tendencies, with smooth transitions between these clusters.

volume fraction target of 0.6 under the assumption of isotropic material. We threshold the coarse scale design such that only pixels with a volume fraction higher than 0.2 are activated in the subsequent fine-scale optimization. The total number of active cells for this example is 132. We compute the principal strain ϵ_{max} and ϵ_{min} from the displacement and use the orientation to design the fine-scale structure. The principal strain is plotted in Figure 10 (b) where regions with similar orientation and maximum to minimum strain can be seen.

In the fine-scale optimization, we map the maximum and minimum principal strain to the stiffness tensor E_{11} and E_{22} as follows:

$$E_{11} = 1.0, E_{22} = 0.6 \frac{\epsilon_{min}}{\epsilon_{max}} + 0.4 \quad (10)$$

The resolution for each cell is 20×20 with a uniform volume fraction target of 0.4 across all cells. We run a total of 400 epochs which takes 17 minutes. The converged multi-scale structure is shown in Figure 10 (c). We can observe a good correlation between the fine-scale structure and the orientation of the stiffness field. The fine-scale structures show clustering behavior, while the transition between the clusters is smooth.

5 LIMITATIONS AND FUTURE WORK

In this study, our primary emphasis lies in showcasing our capability to generate interconnected microstructures amidst demanding design constraints. In the multi-scale topology optimization example, we rely on a mapping between the principal strain and the stiffness tensor. The use of isotropic material in coarse-scale optimization is also not a realistic representation of the stiffness of fine-scale structures. A wide variety of future work can be performed to expand the

application of our proposed approach. Regarding the fine-scale optimization, we could change the objective function such that it becomes a stiffness tensor-constrained volume fraction minimization problem. This allows us to design the desired stiffness tensor from the coarse scale while optimizing fine-scale microstructure to achieve it.

The convergence of the multi-scale structure can be further explored. The examples in the paper, similar to full batch in machine learning, we simultaneously optimize all cells every epoch. However, a mini-batch can also be used such that a selection of cells is optimized. Future works could focus on exploring how to select the correct batch given the convergence of the problem to more effectively optimize multi-scale structures. Once the efficiency is improved, larger size problems with more cell count and extension to 3D can be explored. In a prior work [9], the authors explored using a conditioning field to speed up convergence on single-scale topology optimization problems. The use of a conditioning field can also be applied to multi-scale structures. One possible conditioning field is the rank-N laminates. Where the neural network can help with connecting the Rank-N laminates. In another prior work, [30], Physics Informed Neural Network (PINN) is used to directly optimize topology. It is worth exploring if PINN can also be used in multi-scale optimization, whether in coarse-scale designing stiffness tensors or in fine-scale designing microstructures.

Manufacturing constraints can also be explored. In prior works [31], the neural network-based topology optimization allows the computation of density gradients therefore overhang control can be applied for additive manufacturing. Overhang control can also be applied to microstructures such that each individual cell can be additively manufactured without suffering from local print failures. Multi-material, and multi-physics can also be integrated into the proposed approach.

6 CONCLUSIONS

In conclusion, our study introduces a novel approach to direct multi-scale topology optimization with neural networks. Through the utilization of neural networks, particularly in inverse homogenization tasks, we have effectively enhanced microstructure compatibility within challenging design conditions. Our methodology involves training a topology neural network on a per-case basis, enabling the representation of diverse microstructure designs across the design domain. We demonstrated the efficacy of the approach with examples. Notably, our approach enables the optimization of individual microstructure cells based on specified elasticity tensors while accommodating rotation, thereby facilitating a high degree of design flexibility.

Acknowledgment

This research was funded by Lockheed Martin Corporation MRA19001RPS004.

References

- [1] Zhenguo Nie, Tong Lin, Haoliang Jiang, and Levent Burak Kara. Topologygan: Topology optimization using generative adversarial networks based on physical fields over the initial domain. *Journal of Mechanical Design*, 143(3), 2021.
- [2] François Mazé and Faez Ahmed. Diffusion models beat gans on topology optimization. In *Proceedings of the AAAI conference on artificial intelligence*, volume 37, pages 9108–9116, 2023.
- [3] Amin Heyrani Nobari, Giorgio Giannone, Lyle Regenwetter, and Faez Ahmed. Nito: Neural implicit fields for resolution-free topology optimization. *arXiv preprint arXiv:2402.05073*, 2024.
- [4] Baotong Li, Congjia Huang, Xin Li, Shuai Zheng, and Jun Hong. Non-iterative structural topology optimization using deep learning. *Computer-Aided Design*, 115:172–180, 2019.
- [5] Sangeun Oh, Yongsu Jung, Seongsin Kim, Ikjin Lee, and Namwoo Kang. Deep generative design: Integration of topology optimization and generative models. *Journal of Mechanical Design*, 141(11):111405, 2019.
- [6] Aaditya Chandrasekhar and Krishnan Suresh. Tounn: Topology optimization using neural networks. *Structural and Multidisciplinary Optimization*, 63, 2021.
- [7] Aaditya Chandrasekhar and Krishnan Suresh. Multi-material topology optimization using neural networks. *CAD Computer Aided Design*, 136, 2021.
- [8] Aaditya Chandrasekhar and Krishnan Suresh. Length scale control in topology optimization using fourier enhanced neural networks. *CoRR*, abs/2109.01861, 2021.

-
- [9] Hongrui Chen, Aditya Joglekar, and Levent Burak Kara. Topology Optimization Using Neural Networks With Conditioning Field Initialization for Improved Efficiency. *Journal of Mechanical Design*, 146(6):061702, 12 2023.
- [10] Saketh Sridhara, Aaditya Chandrasekhar, and Krishnan Suresh. A generalized framework for microstructural optimization using neural networks. *Materials & Design*, 223:111213, 2022.
- [11] Jonas Zehnder, Yue Li, Stelian Coros, and Bernhard Thomaszewski. Ntopo: Mesh-free topology optimization using implicit neural representations. *Advances in Neural Information Processing Systems*, 34:10368–10381, 2021.
- [12] Jun Wu, Ole Sigmund, and Jeroen P Groen. Topology optimization of multi-scale structures: a review. *Structural and Multidisciplinary Optimization*, 63:1455–1480, 2021.
- [13] Olivier Pantz and Karim Trabelsi. A post-treatment of the homogenization method for shape optimization. *SIAM Journal on Control and Optimization*, 47(3):1380–1398, 2008.
- [14] Eric Garner, Helena MA Kolken, Charlie CL Wang, Amir A Zadpoor, and Jun Wu. Compatibility in microstructural optimization for additive manufacturing. *Additive Manufacturing*, 26:65–75, 2019.
- [15] Pai Liu, Zhan Kang, and Yangjun Luo. Two-scale concurrent topology optimization of lattice structures with connectable microstructures. *Additive Manufacturing*, 36:101427, 2020.
- [16] Ole Sigmund. Materials with prescribed constitutive parameters: an inverse homogenization problem. *International Journal of Solids and Structures*, 31(17):2313–2329, 1994.
- [17] MP Bendsøe and N Kikuchi. Generating optimal topologies in structural design using a homogenization method, comp. *Meths. Appl. Mech. Engng*, 71:197–224, 1988.
- [18] Martin P Bendsøe. Optimal shape design as a material distribution problem. *Structural optimization*, 1:193–202, 1989.
- [19] M Zhou and GIN Rozvany. The coc algorithm, part ii: Topological, geometrical and generalized shape optimization. *Computer methods in applied mechanics and engineering*, 89(1-3):309–336, 1991.
- [20] Fernando V Senhora, Emily D Sanders, and Glaucio H Paulino. Optimally-tailored spinodal architected materials for multiscale design and manufacturing. *Advanced Materials*, 34(26):2109304, 2022.
- [21] Bo Zhu, Mélina Skouras, Desai Chen, and Wojciech Matusik. Two-scale topology optimization with microstructures. *ACM Transactions on Graphics (TOG)*, 36(4):1, 2017.
- [22] Hao Deng and Albert C To. Topology optimization based on deep representation learning (drl) for compliance and stress-constrained design. *Computational Mechanics*, 66(2):449–469, 2020.
- [23] Hao Deng and Albert C To. A parametric level set method for topology optimization based on deep neural network. *Journal of Mechanical Design*, 143(9), 2021.
- [24] Hau T Mai, Dai D Mai, Joowon Kang, Jaewook Lee, and Jaehong Lee. Physics-informed neural energy-force network: a unified solver-free numerical simulation for structural optimization. *Engineering with Computers*, pages 1–24, 2023.
- [25] Stephan Hoyer, Jascha Sohl-Dickstein, and Sam Greydanus. Neural reparameterization improves structural optimization. *arXiv preprint arXiv:1909.04240*, 2019.
- [26] Zeyu Zhang, Yu Li, Weien Zhou, Xiaoqian Chen, Wen Yao, and Yong Zhao. Tonr: An exploration for a novel way combining neural network with topology optimization. *Computer Methods in Applied Mechanics and Engineering*, 386:114083, 2021.
- [27] Liang Xia and Piotr Breitkopf. Design of materials using topology optimization and energy-based homogenization approach in matlab. *Structural and multidisciplinary optimization*, 52(6):1229–1241, 2015.
- [28] Diederik P Kingma and Jimmy Ba. Adam: A method for stochastic optimization. *arXiv preprint arXiv:1412.6980*, 2014.
- [29] Zvi Hashin and Shmuel Shtrikman. A variational approach to the theory of the elastic behaviour of multiphase materials. *Journal of the Mechanics and Physics of Solids*, 11(2):127–140, 1963.
- [30] Aditya Joglekar, Hongrui Chen, and Levent Burak Kara. Dmf-tonn: Direct mesh-free topology optimization using neural networks, 2023.
- [31] Hongrui Chen, Aditya Joglekar, Kate S Whitefoot, and Levent Burak Kara. Concurrent build direction, part segmentation, and topology optimization for additive manufacturing using neural networks. *Journal of Mechanical Design*, 145(9), 2023.